Research article Available online www.ijsrr.org ISSN: 2279–0543

International Journal of Scientific Research and Reviews

Molecular structure, spectroscopic characteristics, electron density analysis of an organic N-ethyl-N-(2,4,6-trinitrophenyl) nitramide energetic molecule

V. Anbu[1,*] and K.A. Vijayalakshmi[2,*]

[1]Research and Development Centre, Bharathiar University, Coimbatore, 641046, India
[2]Department of Physics, Sri Vasavi College, Erode, 638 316, India.
Email: kavijayalakshmi@yahoo.co.in

ABSTRACT

The molecular structure of an energetic molecule N-ethyl-N-(2,4,6-trinitrophenyl)nitramide (ETNPN) and its spectroscopic properties are analyzed by density functional theory. The calculated IR and Raman spectral bands were discussed with the aid of normal coordinate analysis (NCA) of force field calculations based on DFT method. The intra-molecular charge transfer interactions and stability of the ETNPN molecule were analyzed by the natural bond orbital study. The chemical reactive sites of the molecule were investigated using HOMO-LUMO and molecular electrostatic surface map. In addition, the nonlinear properties of the molecule have been determined using first order hyper polarizability.

KEYWORDS: Nitramide derivative, Vibrational spectra, Molecular orbitals, Electron density, NLO properties

***Corresponding authors:**

V. Anbu

Research and Development Centre,

Bharathiar University,

Coimbatore, 641046, India

v.anbuvee@gmail.com

1. INTRODUCTION

Nonlinear optics (NLO) is a very important phenomenon in the field of photonics that plays a vital role in the area of frequency mixing, optical communications, laser technologies, optical data storage devices, optical image processing, and biomedical applications.[1-4] Organic NLO materials having large second and third-order optical nonlinearities and fast response in technological developments, as well as these materials, are very efficient for Terahertz generation and noise detection.[5-7] The structure of organic NLO materials is based on the π bond system; due to the overlap of π orbital's, delocalization of electronic charge distribution of an aromatic ring leads to the high mobility of the electron density. The design of efficient organic NLO materials mostly relies on a push-pull mechanism that contains an electron-donating group (donor) interacting with an electron-withdrawing group (acceptor) through π-conjugation.[8-11]

In this paper, the N-ethyl-N-(2,4,6-trinitrophenyl) nitramide (ETNPN) molecule was optimized and its spectroscopic bands are analyzed with help of normal coordinate analysis and functional groups are assigned by potential energy distribution. The natural bond orbital, frontier molecular orbital, molecular electrostatic potential and hyperpolarizability of ETNPN molecule were investigated. These studies on ETNPN have been reported for the first time and discussed in detail.

2. COMPUTATIONAL DETAILS

The ETNPN molecule was investigated by quantum chemical density functional theory calculations employing B3LYP/6-311++G(d,p) basis set using the Gaussian 09 program package.[12] The ETNPN molecule was optimized and the optimized structure was used for entire calculations. The (3N-6) modes of vibrations are analyzed and assigned with help of potential energy distribution using Gar2ped program.[13] Natural bond orbital analysis of the molecule was performed using NBO 3.1 program.[14] The ETNPN molecular structure, HOMO-LUMO, and MEP surface were mapped using Gauss View 5.0 visualization program.[15]

3. RESULT AND DISCUSSION

3.1. Optimized parameters

The optimized structural parameters of ETNPN with atom numbering scheme are shown in **Figure 1** and the optimized structural parameters are calculated using the B3LYP/6-311++G(d,p) method are listed in **Table 1**. The theoretically predicted bond lengths of C1-C6, C5-C6 are 1.399, 1.392 Á which are greater than the other C-C bond distance (~1.38 Á) due to the substitution of NO_2 and ethyl group. The π conjugation interaction between N-O and C-C, C-C and C-C bond orbital causes expansion of C2-C1-C6 (122.40°), C2-C3-C4 (122.38°), C4-C5-C6 (123.32°) bond angles

over the other C1-C2-C3 (118.13°), C3-C4-C5 (117.36°), C1-C6-C5 (116.29°) angles of benzene ring.

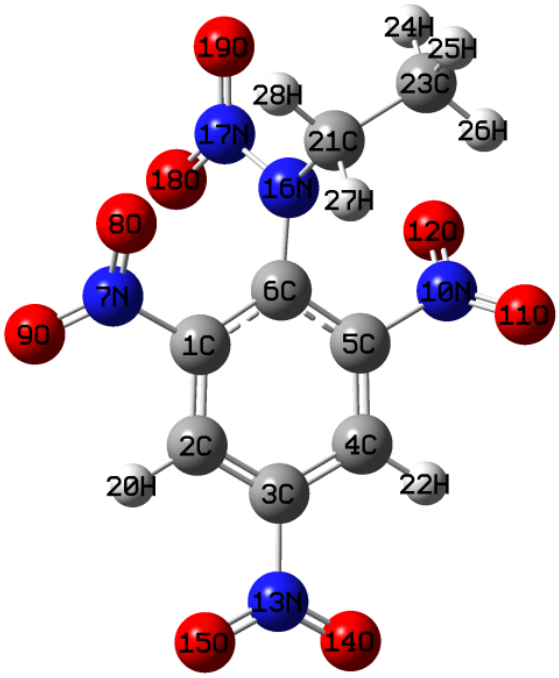

Figure 1. The optimized molecular structure of ETNPN.

The carbon atom of the benzene ring attached nitrogen, C-N bond distances are calculated to be 1.478, 1.481 and 1.475 Á for C1-N7, C3-N13, and C5-N10, respectively. In the NO_2 group, the computed unequal value of the bond length of N=O which indicates the asymmetric charge distribution along the O=N=O bond in the ETNPN molecule. Also, the calculated bond distance of N7-O9, N10-O12, N13-O15, N17-O19 are contracted about ~0.003 Á over the bond distance of N7-O8, N10-O11, N13-O14, N17-O18 due to the influence of one of the oxygen atom of the nitro group. The O=N=O bond angles were calculated to be 126.04° for O8=N7=O9, 126.57° for O11=N10=O12, 125.98° for O14=N13=O15 and 127.05° for O18=N17=O19. The observed dihedral angles of the benzene ring, C6-C1-C2-C3 (-2.74°), C2-C1-C6-C5 (-1.01°), C1-C2-C3-C4 (-1.49°), C2-C3-C4-C5 (-1.41°), C3-C4-C5-C6 (-2.81°) and C4-C5-C6-C1 (-2.11°) are confirmed the co-planar orientation of the ETNPN molecule.

Table 1. Optimized geometric parameters of ETNPN by using B3LYP/6-311++G(d,p) level.

Bond Lengths	B3LYP (Å)	Bond angles	B3LYP (°)	Dihedral Angles	B3LYP (°)
C1-C2	1.380	C2-C1-C6	122.40	C6-C1-C2-C3	-2.74
C1-C6	1.399	C2-C1-N7	116.65	C6-C1-C2-H20	-177.94
C1-N7	1.478	C6-C1-N7	120.94	N7-C1-C2-C3	-177.22
C2-C3	1.383	C1-C2-C3	118.13	N7-C1-C2-H20	2.09
C2-H20	1.082	C1-C2-H20	120.81	C2-C1-C6-C5	-1.01
C3-C4	1.380	C3-C2-H20	121.06	C2-C1-C6-N16	-178.35
C3-N13	1.481	C2-C3-C4	122.38	N7-C1-C6-C5	178.95
C4-C5	1.382	C2-C3-N13	118.83	N7-C1-C6-N16	1.61
C4-H22	1.082	C4-C3-N13	118.79	C2-C1-N7-O8	145.35
C5-C6	1.392	C3-C4-C5	117.36	C2-C1-N7-O9	-32.91
C5-N10	1.475	C3-C4-H22	121.09	C6-C1-N7-O8	-34.61
C6-N16	1.410	C5-C4-H22	121.53	C6-C1-N7-O9	147.12
N7-O8	1.213	C4-C5-C6	123.32	C1-C2-C3-C4	-1.49
N7-O9	1.208	C4-C5-N10	117.07	C1-C2-C3-N13	178.37
N10-O11	1.214	C6-C5-N10	119.61	H20-C2-C3-C4	179.20
N10-O12	1.208	C1-C6-C5	116.29	H20-C2-C3-N13	-0.94
N13-O14	1.211	C1-C6-N16	124.40	C2-C3-C4-C5	-1.41
N13-O15	1.208	C5-C6-N16	119.25	C2-C3-C4-H22	179.71
N16-N17	1.383	C1-N7-O8	117.22	N13-C3-C4-C5	178.74
N16-C21	1.471	C1-N7-O9	116.72	N13-C3-C4-H22	-0.15
N17-O18	1.216	O8-N7-O9	126.04	C2-C3-N13-O14	178.69
N17-O19	1.207	C5-N10-O11	116.20	C2-C3-N13-O15	-1.39
C21-C23	1.521	C5-N10-O12	117.29	C4-C3-N13-O14	-1.45
C21-H27	1.092	O11-N10-O12	126.51	C4-C3-N13-O15	178.47
C21-H28	1.091	C3-N13-O14	116.98	C3-C4-C5-C6	-2.89
C23-H24	1.090	C3-N13-O15	117.04	C3-C4-C5-N10	-176.41
C23-H25	1.093	O14-N13-O15	125.98	H22-C4-C5-C6	-177.84
C23-H26	1.092	C6-N16-N17	116.31	H22-C4-C5-N10	2.46
		C6-N16-C21	121.73	C4-C5-C6-C1	-2.11
		N17-N16-C21	118.65	C4-C5-C6-N16	175.37
		N16-N17-O18	116.42	N10-C5-C6-C1	177.58
		N16-N17-O19	116.53	N10-C5-C6-N16	-4.93
		O18-N17-O19	127.05	C4-C5-N10-O11	-54.16
		N16-C21-H27	105.46	C6-C5-N10-O11	126.13
		N16-C21-H28	107.25	C6-C5-N10-O12	-54.86
		C23-C21-H27	111.29	C1-C6-N16-N17	-66.22
		C23-C21-H28	111.60	C1-C6-N16-C21	92.96
		H27-C21-H28	107.23	C5-C6-N16-N17	116.51
		C21-C23-H24	110.72	C5-C6-N16-C21	-84.31
		C21-C23-H25	108.90	C6-N16-N17-O18	-8.13
		C21-C23-H26	111.94	C6-N16-N17-O19	172.89
		H24-C23-H25	108.32	C21-N16-N17-O18	-167.97
		H24-C23-H26	108.93	C21-N16-N17-O19	13.05
		H25-C23-H26	107.92	C6-N16-C21-C23	116.44
				C6-N16-C21-H27	-5.70
				C6-N16-C21-H28	-119.76
				N17-N16-C21-C23	-84.85
				N17-N16-C21-H27	153.00
				N17-N16-C21-H28	38.95
				N16-C21-C23-H24	58.68
				N16-C21-C23-H25	177.68
				N16-C21-C23-H26	-63.08
				H27-C21-C23-H24	177.54

				H27-C21-C23-H25	-63.47
				H27-C21-C23-H26	55.78
				H28-C21-C23-H24	-62.72
				H28-C21-C23-H25	56.27
				H28-C21-C23-H26	175.52

3.2. NBO analysis

Natural bond orbital (NBO) analysis, the second order perturbation theory analysis of Fock matrix gives the donor-acceptor intra molecular interactions, hybridization, and delocalization of electron occupancy within the molecule. NBO analysis of the title compound was performed using NBO 3.1 program[14] as implemented at the DFT/B3LYP/6-311++G(d,p) level of theory. The important donor-acceptor charge transfer interaction and their stabilization energies, occupancies are listed in **Table 2**. The most strong hyperconjugative interaction of n_3O8→π*(N7-O9), n_3O11→π*(N10-O12) and n_3O14→π*(N13-O15) have maximum stabilization energies of 1034.64, 994.95 and 1078.69 kJ/mol respectively, the respective π* anti bonding orbital with the electron density up to 0.581e, 0.571e and 0.599e. The strong n→σ* hyperconjugative interaction between the oxygen and as well as nitrogen lone pairs and the anti-bonding orbitals of the N-O bonds by the energetic stabilizations of n_2O8→σ*(N7-O9), n_2O9→σ*(N7-O8), n_2O11→σ*(N10-O12), n_2O12→σ*(N10-O11), n_2O15→σ*(N13-O14), n_2O19→σ*(N17-O18), n_3O18→σ*(N17-O19) and n_2O16→σ*(N17-O19) have high stabilization energies of 99.48, 101.95, 97.97, 101.28, 100.40, 100.78, 95.12,444.89 and 151.23 kJ/cal respectively, with the low occupancy up to 0.059e, 0.062e, 0.064e, 0.059e, 0.053e, 0.053e, 0.054e and 0.524e for the respective σ* anti bonding orbital. The intra molecular interaction are formed by the orbital overlap between π(C-C)→π*(C-C) interactions, i.e., π(C1-C2)→π*(C3-C4), π(C1-C2)→π*(C5-C6), π(C3-C4)→π*(C1-C2), π(C3-C4)→π*(C5-C6), π(C5-C6)→π*(C1-C2) and π(C5-C6)→π*(C3-C4) have the stabilization energies 128.24, 166.17, 157.84, 136.41, 119.87 and 157.76 kJ/cal respectively, which results in intra molecular charge transfer cause stabilization of the molecule. These high intra molecular stabilization energies are due to ICT interactions stabilize the molecule.

Table 2. Second order perturbation theory analysis of Fock matrix in NBO basis including the stabilization energies using DFT/B3LYP/6-311++G(d,p) level.

Donor(i)	ED(i)	Acceptor(j)	ED(*j*)	E(2)[a]	E(*j*)-E(*i*)[b]	F(i,j)c
	(e)		(e)	(kJ/mol)	(a.u)	(a.u)
σ(C1-C2)	1.969	σ*(C1-C6)	0.038	23.91	1.45	0.081
σ(C1-C2)		σ*(C3-N13)	0.111	18.51	1.18	0.066
σ(C1-C2)		σ*(C6-N16)	0.033	17.00	1.31	0.065
π(C1-C2)	1.636	π*(C3-C4)	0.335	128.24	0.4	0.1
π(C1-C2)		π*(C5-C6)	0.370	166.17	0.39	0.112
π(C1-C2)		π*(N7-O9)	0.581	83.19	0.26	0.068
σ(C1-C6)	1.968	σ*(C1-C2)	0.019	23.28	1.48	0.081
σ(C1-C6)		σ*(C5-C6)	0.035	17.88	1.46	0.071
σ(C1-C6)		σ*(C5-N10)	0.102	17.29	1.18	0.063
σ(C2-C3)	1.973	σ*(C1-N7)	0.106	17.75	1.18	0.064
σ(C2-C3)		σ*(C3-C4)	0.021	22.44	1.48	0.08
σ(C2-H20)	1.970	σ*(C1-C6)	0.038	22.78	1.24	0.073
σ(C2-H20)		σ*(C3-C4)	0.021	20.22	1.27	0.07
σ(C3-C4)	1.972	σ*(C2-C3)	0.021	22.23	1.48	0.079
σ(C3-C4)		σ*(C5-N10)	0.102	18.88	1.18	0.066
π(C3-C4)	1.637	π*(C1-C2)	0.313	157.84	0.41	0.112
π(C3-C4)		π*(C5-C6)	0.370	136.41	0.39	0.101
π(C3-C4)		π*(N13-O15)	0.599	109.44	0.25	0.077
σ(C4-C5)	1.968	σ*(C3-N13)	0.111	19.13	1.18	0.067
σ(C4-C5)		σ*(C5-C6)	0.035	23.91	1.46	0.082
σ(C4-H22)	1.971	σ*(C2-C3)	0.021	19.93	1.27	0.07
σ(C4-H22)		σ*(C5-C6)	0.035	22.02	1.25	0.073
σ(C5-C6)	1.966	σ*(C1-C6)	0.038	17.58	1.46	0.07
σ(C5-C6)		σ*(C1-N7)	0.106	18.13	1.18	0.065
σ(C5-C6)		σ*(C4-C5)	0.019	23.53	1.48	0.082
π(C5-C6)	1.654	π*(C1-C2)	0.313	119.87	0.41	0.098
π(C5-C6)		π*(C3-C4)	0.335	157.76	0.41	0.111
π(C5-C6)		π*(N10-O12)	0.571	44.97	0.28	0.052
π(C5-C6)		σ*(N16-N17)	0.148	23.24	0.7	0.059
π(N7-O9)	1.986	π*(N7-O9)	0.581	23.74	0.47	0.054
π(N10-O12)	1.989	π*(N10-O12)	0.571	22.94	0.48	0.054
π(N13-O15)	1.986	π*(C3-C4)	0.335	20.05	0.6	0.052
π(N13-O15)		π*(N13-O15)	0.599	25.33	0.45	0.055
σ(N17-O19)	1.990	σ*(N17-O19)	0.524	28.89	0.75	0.074
σ(C21-H27)	1.976	σ*(N16-N17)	0.148	22.65	0.93	0.065
σ(C23-H25)	1.982	σ*(N16-C21)	0.033	24.66	0.97	0.068
n1O8	1.981	σ*(C1-N7)	0.106	19.18	1.23	0.068
n2O8	1.896	σ*(C1-N7)	0.106	71.55	0.71	0.098
n2O8		σ*(N7-O9)	0.059	99.48	0.91	0.133
n3O8	1.434	σ*(N7-O8)	0.062	21.19	0.84	0.067
n3O8		π*(N7-O9)	0.581	1034.64	0.23	0.214
n1O9	1.981	σ*(C1-N7)	0.106	19.01	1.22	0.068
n2O9	1.890	σ*(C1-N7)	0.106	76.28	0.7	0.101
n2O9		σ*(N7-O8)	0.062	101.95	0.9	0.134
n1O11	1.981	σ*(C5-N10)	0.102	18.84	1.23	0.068
n2O11	1.893	σ*(C5-N10)	0.102	69.38	0.71	0.097
n2O11		σ*(N10-O12)	0.064	97.97	0.91	0.131
n3O11	1.431	π*(N10-O12)	0.571	994.95	0.23	0.211

n1O12	1.981	σ*(C5-N10)	0.102	18.88	1.23	0.068
n1O12		σ*(N10-O11)	0.059	14.61	1.42	0.064
n2O12	1.890	σ*(C5-N10)	0.102	73.14	0.71	0.099
n2O12		σ*(N10-O11)	0.059	101.28	0.9	0.134
n1O14	1.982	σ*(C3-N13)	0.111	19.09	1.22	0.068
n2O14	1.895	σ*(C3-N13)	0.111	74.36	0.7	0.1
n2O14		σ*(N13-O15)	0.053	100.40	0.91	0.134
n3O14	1.435	π*(N13-O15)	0.599	1078.69	0.22	0.213
n1O15	1.982	σ*(C3-N13)	0.111	19.13	1.22	0.068
n2O15	1.895	σ*(C3-N13)	0.111	74.78	0.7	0.1
n2O15		σ*(N13-O14)	0.053	100.78	0.91	0.134
n1N16	1.750	σ*(C1-C6)	0.038	41.03	0.96	0.091
n1N16		σ*(C5-C6)	0.035	27.00	0.96	0.074
n1N16		σ*(N17-O19)	0.524	151.23	0.41	0.117
n1N16		π*(N17-O19)	0.193	24.66	0.76	0.061
n1N16		σ*(C21-C23)	0.012	20.77	0.85	0.062
n1N16		σ*(C21-H28)	0.018	15.37	0.86	0.053
n2O18	1.875	σ*(N16-N17)	0.148	110.36	0.69	0.121
n2O18		σ*(N17-O19)	0.524	40.36	0.41	0.063
n2O18		π*(N17-O19)	0.193	88.13	0.76	0.115
n3O18	1.519	σ*(N17-O19)	0.524	444.89	0.37	0.178
n3O18		π*(N17-O19)	0.193	54.81	0.72	0.093
n1O19	1.981	σ*(N17-O18)	0.054	16.91	1.42	0.068
n2O19	1.870	σ*(N16-N17)	0.148	116.35	0.69	0.124
n2O19		σ*(N17-O18)	0.054	95.12	0.89	0.129

3.3. Vibrational analysis

The ETNPN molecule contains 28 atoms and it has 78 modes of fundamental vibrations are calculated and assigned with help of density functional theory and potential energy distribution. The simulated unscaled, scaled values and its assignments with PED are listed in **Table 3**. The simulated IR and Raman spectra are illustrated in **Figure 2**. The various modes of vibrational assignments of an ethyl group, benzene ring, NO_2, CC, CN, and NN functional groups are analyzed and are discussed in detail.

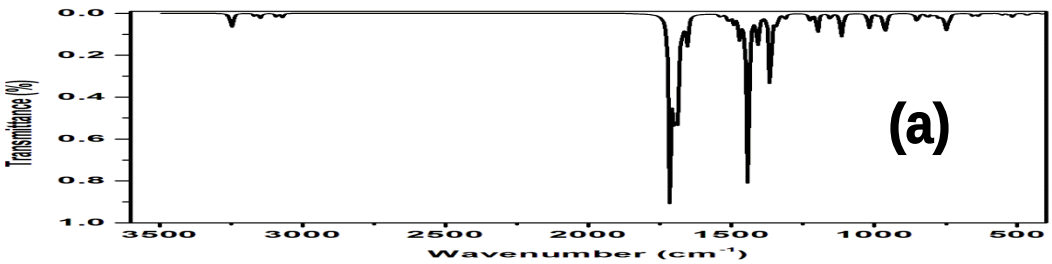

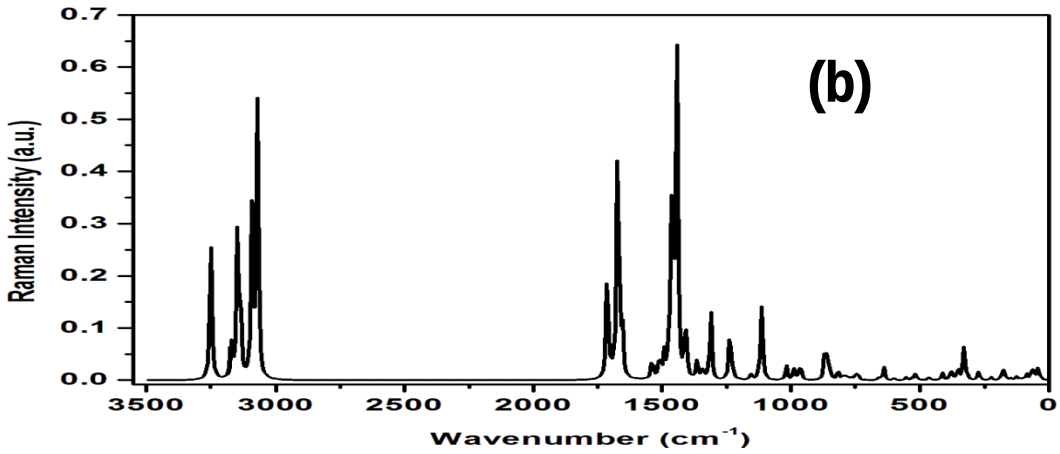

Figure 2. Simulate (a) IR and (b) Raman Spectra of ETNPN

Table 3. Vibrational Assignments of ETNPN

Wavenumber (cm^{-1})		Intensity	[a]Assignments with % of PED
Unscaled	Scaled		
3233	3091	29.82	ν(CH)(99)
3226	3084	22.59	ν(CH)(99)
3151	3017	7.62	$\nu_{as}(CH_3)$(99)
3119	2988	2.51	$\nu_{as}(CH_3)$(99)
3119	2987	12.4	$\nu_{as}(CH_2)$(99)
3074	2947	5.65	$\nu_{s}(CH_3)$(99)
3050	2925	18.45	$\nu_{s}(CH_2)$(99)
1652	1622	357.24	ν(CC)(31) + νas(NO_2)(19) + νs(NO_2)(8)
1647	1617	73.99	ν(CC)(43) + νas(NO_2)(16) + β(CCC)(4)
1638	1608	392.32	$\nu_{as}(NO_2)$(42) + $\nu_{s}(NO_2)$(31)
1615	1587	101.2	$\nu_{as}(NO_2)$(44) + $\nu_{s}(NO_2)$(41)
1607	1579	153.84	$\nu_{as}(NO_2)$(32) + $\nu_{s}(NO_2)$(31) + ν(CC)(15)
1592	1565	150.43	$\nu_{as}(NO_2)$(27) + $\nu_{s}(NO_2)$(26) + ν(CC)(22) + β(CCC)(5)
1513	1488	3.72	$\delta(CH_3)$(83) + $\beta(NO_2)$(9)
1492	1468	8.15	$\delta(CH_3)$(86) + $\beta(NO_2)$(8)
1487	1464	18.69	$\gamma(CH_2)$(22) + ν(CC)(20) + $\delta(CH_3)$(16) + ν(CN)(11)
1475	1452	23.07	$\gamma(CH_2)$(66) + ν(CC)(8) + $\beta(CH_3)$(3) + ν(CN)(3)
1429	1408	4.58	ν(CC)(45) + $\beta(CH_3)$(22) + β(CCN)(13) + ν(CN)(5)
1418	1398	22.2	$\beta(CH_3)$(77) + β(NCC)(10) + ν(CH)(9)
1403	1383	43.62	$\nu_{s}(NO_2)$(45) + β(NHC)(14) + $\beta(NO_2)$(11) + ν(CN)(10)
1394	1374	80.27	β(NCC)(49) + $\nu_{s}(NO_2)$(17) + $\beta(CH_3)$(14) + ν(CN)(4)
1377	1358	165.59	$\nu_{s}(NO_2)$(57) + $\beta(NO_2)$(10) + ν(CN)(8) + β(NHC)(6)
1370	1351	274.97	$\nu_{s}(NO_2)$(37) + $\nu_{as}(NO_2)$(21) + $\beta(NO_2)$(14) + ν(CN)(10) + $\omega(CH_3)$(5)
1367	1348	99.77	ω(CH3)(39) + $\nu(NO_2)$(23) + ν(CN)(9) + $\beta(NO_2)$(4)

1334	1317	9.4	ν_s(NO2)(47) + ω(CH3)(16) + β(NO_2)(10) + β(NCH)(5)
1309	1292	208.74	ν(CN)(34) + ν(NO_2)(11) + β(HCH)(20) + β(NCN)(4)
1266	1250	87.37	ν(CC)(85) + β(CCN)(3)
1210	1197	12.07	Γ(CH_2)(58) + ν(CN)(17) + β(CNC)(10)
1191	1178	14.77	ν(CN)(32) + β(CCC)(25) + ν(CC)(18) + β(CCH)(4)
1156	1144	9.78	ρ(CH_2)(58) + β(CCC)(8) + ν(CN)(8) + β(CCN)(4)
1116	1106	30.34	ρ(CH_2)(34) + ν(CN)(15) + β(NCH)(8) + ν(CH)(6) + β(CHC)(5) + β(CCN)(5)
1103	1092	47.21	β(CCH)(31) + ν(CC)(19) + ρ(CH2)(11) + ν(CH)(8)
1072	1062	55.19	ν(CN)(27) + ν(CH)(21) + β(CCC)(13) + ν(NN)(8) + β(CNC)(4) + ν(CC)(3)
971	964	20.75	ν(CH)(38) + ρ(CH2)(22) + β(CNC)(11) + ν(NN)(9)
960	953	81.25	ν(NN)(22) + β(CCC)(17) + ν(CN)(11) + β(NO_2)(9) + ρ(CH2)(4)
952	946	1.3	δ(CH)(81) + γ(CCCC)(7) + γ(NCCC)(5)
941	935	25.97	δ(CH)(62) + γ(CCCC)(17) + γ(NCCC)(5)
935	929	25.27	ν(CN)(28) + γ(NO_2)(20) + γ(HCCC)(12) + ν(NN)(5) + β(CCC)(4) + τ(CCCC)(3)
927	921	20.92	ν(CN)(34) + γ(NO_2)(28) + β(CCC)(5) + ν(CH)(3)
844	840	7.41	γ(NO_2)(77) + β(CCC)(6)
835	831	28.82	γ(NO_2)(30) + β(HCH)(19) + γ(NCCC)(7) + τ(CCCC)(7) + β(CNC)(6)
790	787	7.83	γ(NCCC)(28) + τ(CCCC)(25) + γ(COON)(24)
787	784	5.39	β(HCH)(18) + γ(COON)(11) + β(HCH)(9) + γ(NOON)(8) + β(OON)(7)
784	780	1.89	ω(NO_2)(30) + β(CH_2)(22) + γ(NCCC)(12) + β(CNC)(8) + τ(CCCC)(4)
757	755	17.18	ω(NO_2)(60) + γ(COON)(7) + γ(CNCN)(6) + β(CCC)(4)
746	743	26.44	ω(NO_2)(20) + τ(CCCC)(20) + β(CH_2)(11) + γ(NCCC)(11) + γ(COON)(7)
735	732	37.48	ω(NO_2)(36) + β(CCC)(29) + ν(CN)(8) + β(HCH)(4)
725	723	16.4	ω(NO_2)(61) + γ(NCCC)(17) + τ(CCCC)(10)
708	706	4.97	τ(CCCC)(22) + γ(NCCC)(17) + γ(COON)(12) + β(OCN)(5) + β(CCC)(4)
664	663	4.41	β(CCN)(19) + β(OCN)(17) + τ(CCCC)(16) + γ(NCCC)(13) + γ(COON)(6)
603	602	7.54	β(CNN)(25) + β(NCH)(11) + ν(NN)(10) + ω(NO_2)(7) + β(OCN)(6) + τ(CCCC)(6)
573	573	8.52	δ(CCC)(36) + γ(NCCC)(12) + β(OCN)(12) + ρ(NO_2)(8)
545	545	3.76	ρ(NO_2)(51) + β(CCC)(12) + β(CNC)(10)
524	524	8.34	δ(CCC)(42) + γ(NCCC)(31) + ρ(NO_2)(4)
482	483	1.46	ν(NN)(13) + τ(CCCC)(9) + γ(NCCC)(7) + β(OCN)(6) + β(CNC)(6)
469	470	7.41	Rb(CCN)(22) + γ(NCCC)(14) + τ(CCCC)(13) + γ(CNCN)(12) + β(OCN)(6)
410	411	3.54	β(NCH)(23) + τ(CCCC)(17) + γ(CNCN)(10) + γ(NCCC)(9) + ρ(NO_2)(8)
367	368	0.51	τ(CCCC)(29) + β(OCN)(16) + γ(NCCC)(9) + β(CCC)(6) + β(CNC)(5) + ν(CN)(4)
350	351	0.46	β(CCC)(19) + β(CNC)(15) + ρ(OCN)(11) + β(NCN)(11) + ν(CN)(10)
327	328	3.36	β(NCN)(18) + β(CNC)(12) + β(OCN)(12) + γ(CNCN)(6) + τ(CNCH)(5)
321	322	2.46	γ(NCCC)(34) + τ(CCCC)(26) + β(CCN)(10) + β(OCN)(10)
318	319	0.85	ν(CN)(47) + β(CCC)(8) + ν(CC)(6) + β(NO2)(5)
274	275	4.13	β(NCH)(25) + γ(NCCN)(16) + β(CCC)(16) + ν(CN)(14) + β(CNC)(3)
246	247	1.97	β(CNC)(19) + β(NCN)(15) + τ(CNCH)(14) + τ(NCHH)(14) + β(CCC)(7)
197	198	1.7	τ(NCHH)(38) + β(NCN)(21) + τ(CNCH)(7) + β(CCC)(5) + β(CNC)(4)
177	178	4.21	γ(NCCC)(42) + β(CNC)(11) + τ(CCCC)(11) + γ(HCCC)(7) + β(OCN)(6)
170	171	2.15	β(CNC)(28) + τ(CCCC)(11) + τ(NCCC)(8) + τ(CNCC)(7) + β(CNC)(5)

162	163	1.08	β(CNC)(51) + τ(NCCC)(9) + τ(CCCC)(5)
155	156	2.1	β(CNC)(32) + τ(CNCH)(19) + τ(NCHH)(13) + τ(CNCN)(3)
136	137	1.49	τ(CNCH)(49) + β(CNC)(19) + τ(NCHH)(15)
125	126	0.43	τ(CNCN)(53) + τ(CNNO)(13) + τ(CNCH)(12) + β(CNC)(4)
102	102	0.91	τ(CNNO)(67) + τ(CNCH)(5) + β(HNC)(4)
98	99	6.09	τ(NCCC)(60) + τ(CNNO)(9) + τ(CNCH)(6)
65	66	1.44	τ(ONCC)(35) + τ(CNCC)(29) + τ(CNCN)(7)
51	51	1.67	τ(CNCC)(41) + τ(ONCC)(41)
43	43	0.26	τ(ONCC)(64) + τ(CNCC)(15) + τ(CCCC)(13)
40	40	0.32	τ(CCCC)(45) + τ(ONCC)(19) + β(CCN)(8) + τ(NCCC)(8) + τ(CNCN)(6)
33	33	0.19	τ(ONCC)(64) + β(CNC)(17) + τ(CNCH)(7)

[a]ν; stretching, β; in-plane bending, γ; out-of-plane bending, rocking, τ; torsion.

3.3.1. Ethyl group vibrations

CH_3 vibration

The ethyl groups CH_3 asymmetric and symmetric stretching wavenumbers are observed between 3000-2960 cm^{-1} and 2970-2840 cm^{-1} respectively.[16,17] The DFT calculated bands at 3017 and 2988 cm^{-1} are attributed to CH_3 asymmetric stretching with PED of 99%, as well as CH_3 symmetric stretching band is calculated at 2947 cm^{-1} with PED of 99%. The CH_3 asymmetric and symmetric deformations are expected in the region 1475-1455 cm^{-1} and 1390-1360 cm^{-1}, respectively.[18] The DFT simulated out of plane CH_3 asymmetric deformation mode at 1488 and 1468 cm^{-1} with PED of 83% and 86% respectively. The predicted band at 1398 cm^{-1} (PED of 77%) is assigned to in plane CH_3 symmetric deformation. The CH_3 wagging and rocking modes are active in the region 1360-1320 cm^{-1}. The CH_3 wagging mode of vibration is computed at 1348 cm^{-1} (PED of 39%) in vibrational spectrum.

CH_2 vibration

The ethyl group, asymmetric and symmetric CH_2 stretching is usually present in the region 2970-2900 cm^{-1} and 2940-2840 cm^{-1} respectively.[16-18] The CH_2 asymmetric and symmetric bands are calculated and assigned at 2987 cm^{-1} and 2925 cm^{-1} respectively. The CH_2 scissoring deformation vibration commonly appears in the region 1480-1420 cm^{-1}.[19,20] In ETNPN, the CH_2 scissoring deformations are calculated at 1464 and 1452 cm^{-1} with PED of 22% and 66% respectively. The CH_2 twisting bands generally appear in the region 1290-1200 cm^{-1}.[18] The CH_2 rocking vibrations are commonly appearing in the region 1190-1060 cm^{-1} and 835-715 cm^{-1} respectively. The vibrational band calculated at 1197 cm^{-1} is assigned to CH_2 twisting with PED of 58%. As well as the bands at 1144, 1106 and 784 cm^{-1} are attributed to CH_2 rocking.

3.3.2. Benzene ring vibration

CH vibration

For the aromatic CH stretching vibrational band can appear in the region 3100–3000 cm^{-1}.[21] The computed peaks at 3091 and 3084 cm^{-1} are attributed to CH stretching of a benzene ring with a PED of 99%. The tetrasubstituted aromatic ring CH in-plane bending and out of plane bending was generally found in the region 1205-1085 cm^{-1} and 965-950 cm^{-1} respectively.[22,23] The CH inplane bending was calculated at 1092 cm^{-1} with PED of 31%. The theoretically calculated bands at 946 and 935 cm^{-1} are attributed to CH out of plane bending vibration with PED of 81% and 62% respectively.

CC vibrations

The vibrational band for CC ring stretching of the NO_2 substituted skeletal benzene ring occurs at 1625-1430 cm^{-1}.[22] The calculated bands at 1622 cm^{-1} (PED of 31%) and 1617 cm^{-1} (PED of 43%) are attributed to aromatic CC stretching vibrations. The phenyl ring CC stretching band commonly occurs in the region 1380-1240 cm^{-1}. The simulated band at 1250 cm^{-1} with PED of 45% is assigned to phenyl CC ring stretching. The benzene ring deformation vibrations due to CCC out of plane bending are occurred at 580-505 cm^{-1}. The CCC out of plane deformation vibration is calculated at 573 and 524 cm^{-1} with PED of 36% and 42% respectively. The ring breathing band due to NO_2 attached C-N stretching generally occurs in the region 540-490 cm^{-1}. The band 470 cm^{-1} is attributed to be ring breathing of C-N stretching. The aromatic ring torsion vibrations are calculated at 368 cm^{-1} with PED of 29%.

3.3.3. NO_2 Vibrations

Aromatic nitro molecules containing strong absorption band owing to the NO_2 asymmetric and symmetric stretching in the regions 1570–1485 cm^{-1} and 1370–1320 cm^{-1} respectively.[23] The calculated asymmetric stretching at 1608, 1587, 1579 and 1565 cm^{-1} with PEDs of 42%, 44%, 32% and 27% respectively. The most intense peaks of the NO_2 symmetric stretching is computed at 1383, 1358, 1351 and 1317 cm^{-1} with PEDs of 45%, 57%, 37%, and 47% respectively. The NO_2 scissoring modes are expected in the region 850±60 cm^{-1}.[21,24,25] The predicted vibrational bands at 840 cm^{-1} (PED of 77%) and 831 cm^{-1} (PED of 30%) are attributed to NO_2 scissoring. Aromatic nitro group wagging and rocking modes are active in the region 740±50 cm^{-1} and 540±50 cm^{-1}, respectively.[26,27] Theoretically calculated bands at 780-723 cm^{-1} and 545 cm^{-1} are owing to NO_2 wagging and rocking respectively.

3.3.4. C-N, C-C, and N-N vibrations

The band for CN stretching modes occurs in the region 1180-865 cm^{-1}.[18,19] The calculated wave numbers at 1178, 1062, 929 and 921 cm^{-1} are assigned for CN stretching with the potential energy distribution of 32%, 27%, 28%, and 34% respectively. The aromatic compound CNN deformation vibrations are commonly occurring near 590 cm^{-1}. The computed band at 602 cm^{-1} is attributed to C-N deformation with PED of 25%. The ethyl group, C-C stretching vibration is calculated at 1408 cm^{-1} with PED of 44%. As well as aromatic azo compound NN stretching vibrations are calculated at 953 cm^{-1}.

3.4. Frontier molecular orbital

Highest occupied molecular orbital (HOMO) act as electron donor and lowest unoccupied molecular orbital (LUMO) act as an electron acceptor are collectively called as frontier molecular orbital, which are very important parameters for quantum chemistry such as the insight into the nature and reactivity of the molecule.[28] The molecular orbital theory is due to the interaction between HOMO and LUMO orbital of a molecular structure, transition state transition of π-π* type is observed. While the E_{HOMO} is directly related to the ionization potential, E_{LUMO} is directly related to the electron affinity. The E_{gap}, the energy difference between the HOMO and LUMO regulates the kinetic stability, chemical reactivity, optical polarizability, and chemical hardness-softness of a molecule is important stability for structures.[29,30] 3D plots of frontier molecular orbital (HOMOs and LUMOs) with the energy values of ETNPN are shown in **Figure 3**. The E_{HOMO} and E_{LUMO} values are -7.670 eV and -2.944 eV respectively, the Egap is 4.726 eV. From the **Figure 3**, it is clear that HOMO is localized on all the NO_2 group except O14-N13-O15, an ethyl group, N16, C5-C6, C1, and C3 atom; LUMO is localized on the entire benzene ring except for C5 atom, O14-N13-O15, O8-N7-O9, N16-N17, O18, O19 and C21 atom of the ethyl group. According to the Koopmann's theorem[31], the ionization energy and electron affinity, electro negativity (χ), chemical reactivity (μ), softness (s) and other calculated reactivity descriptors of PTM molecule are presented in **Table 4**.The E_{HOMO} and E_{LUMO} are corresponding to the approximated values of the ionization potential (IP) and the electron affinity (EA), respectively. The electro negativity, χ is calculated from the relation, χ = (IP+EA)/2 and the negative value of χ gives the chemical potential of the molecular system. The stability of the molecule can be interpreted from the value of chemical hardness (η) by the relation, η = (IP-EA)/2. The η value represents the resistance to polarization due to an external perturbation on the molecular system. The global softness value reflects the degree of chemical reactivity of the molecule and is calculated using the relation, S = 1/2η. The electrophilicity index ($\omega = \mu^2/2\eta$) is considered to be a measure of the electrophilic power which characterizes the energy lowering

associated with the maximum electron flow between donor and acceptor orbitals. The total energy change is calculated from the relation, $\Delta E_T = -\eta/4$. The energy gain or loss in a donor-acceptor charge transfer is determined from the overall energy balance, ΔE= EA-IP. The HOMO-LUMO energy gap is small, it promotes the interaction between HOMO and LUMO and also stabilizes the molecule and thereby NLO activity.

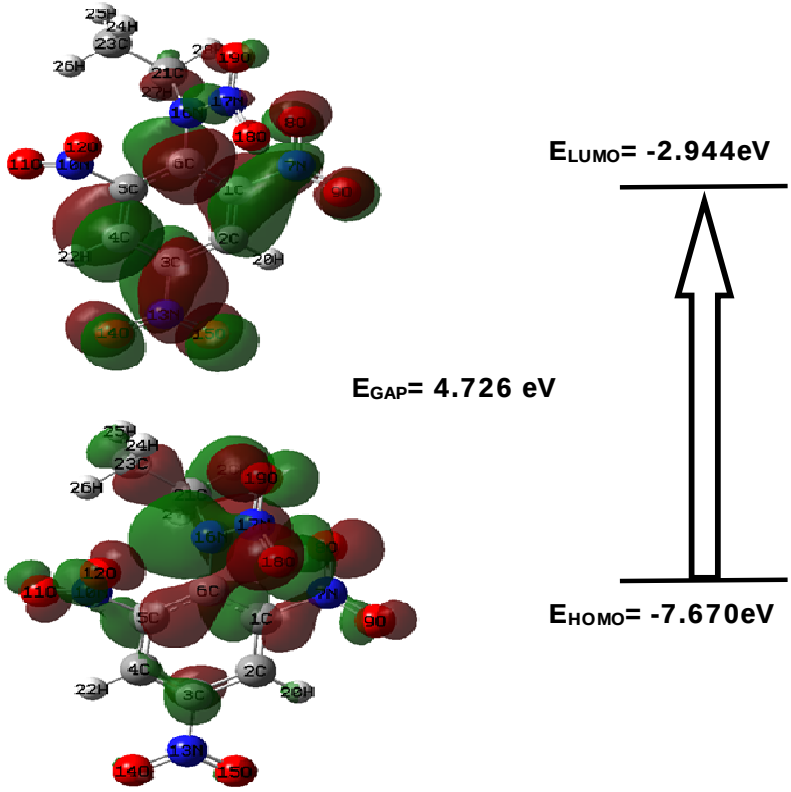

Figure 3. Frontier molecular orbitals of ETNPN.

Table 4. Calculated local reactivity parameters of ETNPN at DFT/B3LYP/6-311++G(d,p) method.

Parameters	B3LYP/6-311++G(d,p)
HOMO energy, E_{HOMO} (eV)	-7.670
LUMO energy, E_{LUMO} (eV)	-2.944
HOMO- LUMO energy gap, ΔE_{GAP} (eV)	4.726
Ionisation potential, IP (eV)	7.670
Electron affinity, EA (eV)	2.944
Electronegativity, χ (eV)	5.307
Chemical hardness, η (eV)	2.363
Global softness, S $(eV)^{-1}$	0.212
Chemical potential, μ (eV)	-5.307
Electrophilicity index, ω (eV)	5.959
Total energy change, ΔE_T (eV)	-0.591
Overall energy balance, ΔE (eV)	-4.726

3.5. Molecular Electrostatic Potential

The molecular electrostatic potential is widely used as reactivity towards electrophilic and nucleophilic attacks as well as hydrogen bonding interactions; it is very useful for studying the physiochemical property relationships of molecular structures.[32,33] The MEP surface for ETNPN was generated by mapping DFT/B3LYP/6-311++G(d,p) method, electrostatic potential onto the molecular electron density surface is shown in **Figure 4**. In **Figure 4**, the dissimilar values of the electrostatic potential at the surface are indicated by different colors, the potential increases in the order of red < yellow < green < blue. In MEP of ETNPN, the isosurface=-0.106a.u. representing the regions that eagerly donate electron (nucleophilic centre) and isosurface= +0.106 a.u. representing the regions that accept electrons (electrophilic center). In MEP surface the maximum positive region, which is preferred site for the nucleophilic attack is depicted as blue, while the maximum negative region is selected site for the electrophilic attack is represented as red. As seen from **Figure 4**, the red region electrophilic reactivity was essentially localized on the oxygen atoms in the nitro group, whereas the blue region nucleophilic reactivity of the molecule was mainly localized on the carbon atoms in the benzene ring and nitrogen.

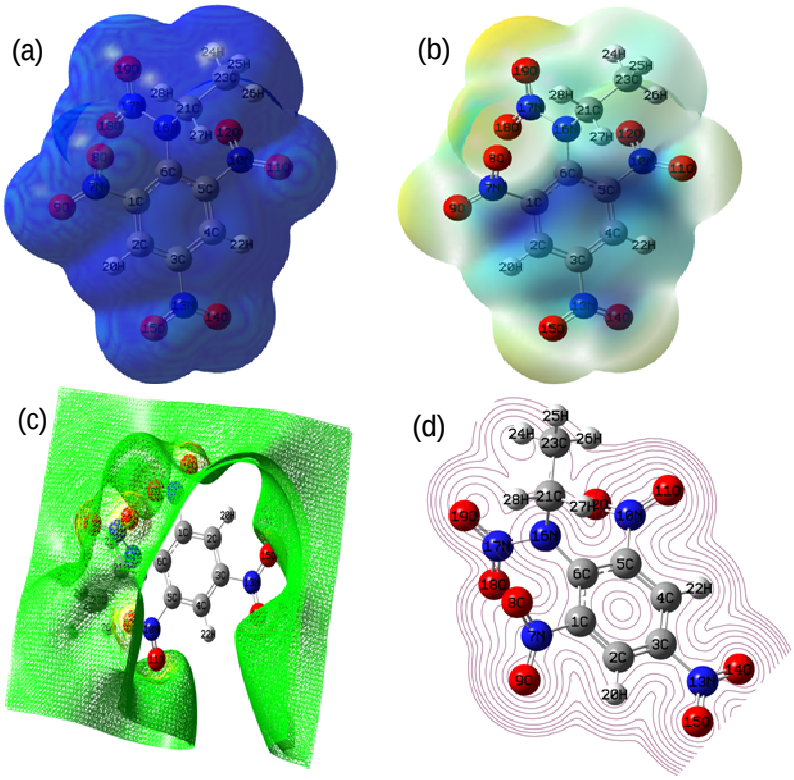

Figure 4.Total electron density (TED), molecular electrostaticpotential (MEP), electrostatic potential contour map and electrostaticpotential (ESP) of ETNPN.

3.6. First order hyperpolarizability

The computed values of nonlinear optical response properties of ETNPN molecule such as the first hyperpolarizability, polarizability, anisotropy of polarizability and total static dipole moment are presented in **Table 5**. Molecules have maximum values of hyperpolarizability, polarizability and dipole moment exhibit significant NLO properties. The DFT calculations, the first order hyperpolarizability value of ETNPN are 7.553 $x10^{-31}$ esu, the mean polarizability value is –1.953 $x10^{-23}$ esu and the anisotropy of polarizability is observed to be 3.531 $x10^{-23}$ esu. Also, the calculated first hyperpolarizability value is 2.02 times that of urea (3.728 $x10^{-31}$ esu) and the computed mean polarizability is 2.7 times that of urea. The high values observed in hyperpolarizability values of βxxy, βxyy and βxzz and polarizability values of αxz and αyz components compare than other components, it is indicate that the strong delocalization of electron cloud in these directions, which illustrates that the charge conjugation is perpendicular to the bond axis and also the substantial involvement of π orbitals in the charge transfer interaction. Thus the high value of hyperpolarizability is attributed to the ICT interactions between donor and acceptor, especially the extent of n→π* conjugation, HOMO–LUMO energies and symmetry of the molecule, which support the NLO activity of the crystal. Another parameter used as a descriptor to represent the charge movement through the molecule is the dipole moment. The dipole moment is an important molecular electronic property which reflects the charge distribution and is given as a vector in three dimensions. The direction of the dipole moment vector in a molecule depends on the centers of positive and negative charges. The large value of the total dipole moment indicates the strong polarity of the bond and it is computed for ETNPN to be 3.7608 Debye, which is 2.73 times that of urea (1.3732 Debye). These high values of molecular dipole moment and polarizability relative to urea show the large NLO property of ETNPN crystal.

Table 5. NLO properties of ETNPN

dipole		Polarizability (esu)		hyperpolarizability (esu)		Second-order hyperpolarizability (esu)	
μx	0.0995	α xx	-137.079	Bxxx	-103.187	γ_{xxxx}	-4842.70
μy	1.5908	α xy	-3.7948	Bxxy	15.0958	γ_{yyyy}	-2434.74
μz	-3.4063	α yy	-136.944	Bxyy	15.7785	γ_{zzzz}	-552.591
μtotal	3.7608	α xz	5.9537	Byyy	0.6111	γ_{xxyy}	-1107.44
		α yz	0.3385	Bxxz	-14.8944	γ_{xxzz}	-764.065
		α zz	-121.457	Bxyz	-3.6679	γ_{yyzz}	-477.359

		α total	-1.9537×10^{-23}	Byyz	-5.3978	γtotal	-1.2621×10^{-26}
		Δ α	3.5317×10^{-23}	Bxzz	5.8764		
				Byzz	-1.5846		
				Bzzz	-7.9286		
				β total	7.55301×10^{-31}		

4. CONCLUSION

The detailed spectroscopic bands have been investigated based on quantum chemical calculation and function groups were assigned using scaled quantum mechanical force field method of the N-ethyl-N-(2,4,6-trinitrophenyl) nitramide molecule. The intra-molecular interactions, stabilization energies and electron density of the title molecule were analyzed using NBO analysis. The HOMO-LUMO energy gap is calculated 4.726 eV, which improves the ICT interactions capable to produce the enhanced NLO responses. The electrophilic and nucleophilic reactivity of the title molecule is analyzed by MESP surface plot. Based on the DFT computations, the hyperpolarizability of the title molecule is calculated 3.531 $\times 10^{-23}$esu, which value is 2.02 times that of urea. The hyperpolarizability values also proposed the better NLO response of the ETNPN molecule.

REFERENCE

1. Azhar SM, Anis M, Hussaini SS, Kalainathan S, Shirsat MD, Rabbani G. Doping effect of l-cystine on structural, UV–visible, SHG efficiency, third order nonlinear optical, laser damage threshold and surface properties of cadmium thiourea acetate single crystal. Opt. Laser Technol. 2017; 87: 11–16.
2. De la Torre G, Vazquez P, Agullo-Lopez F, Torres T. Role of Structral Factors in the Nonlinear Optical Properties of Phthalocyanines and Related Compounds. Chem. Rev. 2004; 104: 3723-3750.
3. inothkumar P, Mohan Kumar R, Jayavel R, Bhaskaran A. Synthesis, growth, structural, optical, thermal and mechanical properties of an organic Urea maleic acid single crystals for nonlinear optical applications. Opt. Laser Tech. 2016; 81: 145–152.
4. Krishnakumar V, Jayaprakash J, Boobas S, Komathi M. Synthesis, growth, optical and anisotropic mechanical behaviour of organic nonlinear optical imidazolium 2-chloro-4-nitrobenzoate single crystals. Eur. Phys. J. Plus 2016; 131: 375–385.
5. Thirupugalmani K, Karthick S, Shanmugam G, Kannan V, Sridhar B, Nehru K, Brahadeeswaran S. Second- and third-order nonlinear optical and quantum chemical studies

on 2-amino-4-picolinium-nitrophenolate-nitrophenol: A phasematchable organic single crystal. Opt. Mater. 2015; 49: 158–170.

6. Brahadeeswaran S, Onduka S, Takagi M, Takahashi Y, Adachi H, Yoshimura M, Mori Y, Sasaki T. Growth of high-quality DAST crystals for THz applications. J. Cryst. Growth 2006; 292: 441–444.
7. Criado A, Dianez MJ, Garrido SPC, Fernandes IM, Belsley ME, M. De Gomes. 1,1,3,3-Tetramethylguanidinium dihydrogenorthophosphate. Acta Cryst. 2000; C56: 888.
8. Zaccaro J, Sulvestrini JP, Ibanez A, Ney P, Fontana MD, Electric-field frequency dependence of Pockels coefficients in 2-amino-5-nitropyridium dihydrogen phosphate organic–inorganic crystals. J. Opt. Soc. Am. B. 2007; 17: 427-432.
9. Brahadeeswaran S, Onduka S, Takagi M, Takahashi Y, Adachi H, Kamimura T, Yoshimura M, Mori Y, Yoshida K, Sasaki T. Twin-free and High-Quality DAST Crystals − Effected through Solutions of Lower Supersaturation Coupled with Isothermal Solvent Evaporation. Cryst. Growth. Des. 2006; 6: 2436–2468.
10. Rodríguez M, Ramos-Ortíz G, Maldonado JL, Herrera-Ambriz VM, Domínguez O, Santillan R, Farfán N, Nakatani K. Structural, thermal and optical characterization of a Schiff base as a new organic material for nonlinear optical crystals and films with reversible noncentrosymmetry. Spectrochimica Acta Part A 2011; 79: 1757–1761.
11. Yavuz M, Tanak H. Density functional modelling studies on *N*-2-Methoxyphenyl-2-oxo-5-nitro-1-benzylidenemethylamine. J. Mol. Struct.: THEOCHEM 2010; 961: 9–16.
12. Frisch MJ, et al., Gaussian 09, Revision A.02, Gaussian Inc., Wallingford, CT, 2009.
13. Martin JML, Van Alsenoy C, GAR2PED: A Program to Obtain a PotentialEnergy Distribution from a Gaussian Archive Record. University of Antwerp, Antwerp, Belgium, 1995.
14. Glendening ED, Reed AE, Carpenter JE, Weinhold F. ‘‘NBO Version 3.1’’, Theoretical Chemistry Institute and Department of Chemistry, University of Wisconsin, Madison, 1998.
15. Dennington RI, Keith T, Millam J, Eppinnett K, Hovell W. Gauss View, Version 3.09, 2003.
16. Bernstein HJ. The average XH stretching frequency as a measure of XH bond properties. Spectrochim. Acta, 1962; 18: 161-170.
17. Ball DF, Goggin PL, McKean DC, Woodward LA. Infra-red and Raman spectra of dimethyl and trimethyl silanes and some deuterated derivatives. Spectrochim. Acta, 1960; 16: 1358-1367.
18. Socrates G. Infrared Characteristic Group Frequencies. Wiley-Inter Science Publication, New York, 1990.

19. Colthup NB, Daly LH, Wiberley SE. Introduction to Infrared and Raman Spectroscopy. Academic press, Inc, London, 1975.
20. McMurry CL, Thornton V. Correlation of Infrared Spectra. Anal. Chem. 1952; 24: 318-334.
21. Varsanyi G. Assignment for vibrational Spectra of Seven Hundred Benzene Derivatives. Academic Kiaclo, Budapest, 1973.
22. Roeges NPG. A Guide to the Complete Interpretation of Infrared Spectra of Organic Structures. Wiley publications, New York, 1994.
23. Smith B. Infrared Spectral Interpretation: A Systematic Approach. CRC Press, Washington, DC, 1999.
24. Rao PM, Rao GR, Vibrational spectra and normal coordinate analysis of monohalogenated nitrobenzenes. J. Raman Spectrosc. 1989; 20: 529–540.
25. Mehdi KC. Vibrational spectra of ortho-, meta- and para-fluoronitrobenzene. Spectrochim. Acta 1964; 20: 675–683.
26. Mooney EF. The infra-red spectra of chloro- and bromobenzene derivatives—II. Nitrobenzenes. Spectrochim. Acta 1964; 20: 1021–1032.
27. Clarkson J. Smith WE. A DFT analysis of the vibrational spectra of nitrobenzene. J. Mol. Struct. 2003; 655: 413–422.
28. Thanikaivelan P, Subramanian V, Raghava Rao J, Nair BU. Application of quantum chemical descriptor in quantitative structure activity and structure property relationship. Chem. Phys. Lett. 2000; 323: 59–70.
29. Lewis DFV, Ioannides C, Parke DV. Interaction of a series of nitriles with the alcohol-inducible isoform of P450: Computer analysis of structure—activity relationships. Xenobiotica 1994; 24: 401–408.
30. Asiri AM, Karabacak M, Kurt M, Alamry KA. Synthesis, molecular conformation, vibrational and electronic transition, isometric chemical shift, polarizability and hyperpolarizability analysis of 3-(4-Methoxy-phenyl)-2-(4-nitro-phenyl)-acrylonitrile: A combined experimental and theoretical analysis. Spectrochim. Acta, Part A, 2011; 82: 444–455.
31. Koopmans TA. About the assignment of wave functions and eigenvalues to the individual electrons of an atom. Physica 1933; 1: 104–113.
32. Politzer P, Truhlar DG. Chemical Application of Atomic and Molecular Electrostatic Potentials. Plenum, New York, 1981.
33. Politzer P, Murray JS. Molecular electrostatic potential and chemical reactivity. Rev. Comp. Chem. 1991; 2: 273–312.